

# AstroClearNet: Deep image prior for multi-frame astronomical image restoration

Yashil Sukurdeep<sup>a,\*</sup>, Fausto Navarro<sup>b</sup>, Tamás Budavári<sup>a,c,d</sup>

<sup>a</sup>*Department of Applied Mathematics and Statistics, Johns Hopkins University, Baltimore, 21218, MD, USA*

<sup>b</sup>*Johns Hopkins University, Baltimore, 21218, MD, USA*

<sup>c</sup>*Department of Computer Science, Johns Hopkins University, Baltimore, 21218, MD, USA*

<sup>d</sup>*Department of Physics and Astronomy, Johns Hopkins University, Baltimore, 21218, MD, USA*

---

## Abstract

Recovering high-fidelity images of the night sky from blurred observations is a fundamental problem in astronomy, where traditional methods typically fall short. In ground-based astronomy, combining multiple exposures to enhance signal-to-noise ratios is further complicated by variations in the point-spread function caused by atmospheric turbulence. In this work, we present a self-supervised multi-frame method, based on deep image priors, for denoising, deblurring, and coadding ground-based exposures. Central to our approach is a carefully designed convolutional neural network that integrates information across multiple observations and enforces physically motivated constraints. We demonstrate the method’s potential by processing Hyper Suprime-Cam exposures, yielding promising preliminary results with sharper restored images.

*Keywords:* deep generative prior, ground-based astronomy, astronomy image processing

---

## 1. Introduction

The latest ground-based astronomical surveys, such as the Hyper Suprime-Cam (HSC) survey [1] and the upcoming Legacy Survey of Space and Time (LSST) from the Rubin Observatory [2], are designed to capture exposures of vast portions of the night sky. These surveys rely heavily on high-resolution ground-based telescopes that produce massive datasets, necessitating substantial processing before meaningful scientific analysis can occur. In particular, imaging distant and faint celestial objects as part of these large-scale surveys requires advanced image processing algorithms to maximize the extraction of reliable and useful information.

A key challenge when developing such algorithms lies in addressing atmospheric blur, an unwanted but inevitable consequence of ground-based observations. The process of mitigating this blur, known as deconvolution, is particularly complex due to the high noise levels, wide dynamic range, and various artifacts present in the exposures. Our work tackles the challenge of multi-frame astronomical image

restoration, focusing on combining multiple noisy and blurry exposures to produce a sharp, unified latent image of the night sky.

### 1.1. Related work

Past approaches for multi-frame image restoration in the field of astronomy include lucky imaging [3], coaddition [4], maximum likelihood estimation [5, 6], and streaming methods [7, 8, 9, 10, 11]. These techniques must carefully balance the effective integration of data from multiple observations, while managing noise levels and blur across exposures.

More recently, several machine learning and deep learning frameworks have achieved viable results in a variety of difficult inverse imaging problems, including image restoration. One such approach involves training a convolutional neural network in a supervised manner to deblur images by performing spatial convolution with a large inverse kernel [12]. Other methods use neural networks to enhance or post-process the outputs of classical image restoration methods, such as Wiener or Richardson-Lucy deconvolution, which rely on undoing the blur in the Fourier domain [13, 14]. These traditional methods

---

\*Corresponding author: Yashil Sukurdeep  
yashil.sukurdeep@jhu.edu

also serve as inspiration for other end-to-end deep learning image restoration techniques [15].

All of these supervised approaches rely on collections of labeled training data, which is a major impediment for their adoption in the field of astronomy, where ground truth observations are costly to acquire. This motivates the need for unsupervised deep learning approaches for astronomical image restoration.

Prominently, the method of *deep image priors*, a self-supervised technique that was introduced by Ulyanov et al. [16], represents one such avenue. As part of this approach, a so-called “hourglass” image generator network is used to parametrize the mapping from a randomly initialized vector to a single degraded image. This mapping can be leveraged to perform a variety of image processing tasks, such as denoising, in-painting, artifact removal, and super-resolution, among others. The framework has been extended to perform blind image deconvolution with natural images [17, 18]. Yet, such techniques remain absent from the astronomy community.

## 1.2. Contributions

Inspired by the aforementioned deep learning approaches for image restoration, and in particular by deep image priors, we develop a novel unsupervised method for multi-frame astronomical image restoration, dubbed *AstroClearNet*. As part of our approach, we solve for a sharp, noise-free latent image of the night sky by using information from multiple noisy and blurry co-registered exposures of a given region of the sky.

In particular, we model the latent image as a *function* of the multiple noisy and blurry exposures, and parametrize this function using a carefully-designed neural network with learnable parameters. By learning the parameters of the network and exploiting the regularizing effect imposed by the network’s architecture, *AstroClearNet* yields a latent image which corresponds to a maximum a posteriori (MAP) estimate for a given statistical model of the exposures, as outlined in Section 3.1.

Our approach is unique in that rather than finding a latent image for a single degraded observation, we combine information from multiple exposures of the same part of the sky in order to generate a single, common latent image. As a result, the neural network architecture proposed in this paper, which is relatively simple and contains few learnable parameters, is suited to processing batches of expo-

sure of the sky, akin to imaging data produced by modern ground-based surveys.

To demonstrate the effectiveness and performance of *AstroClearNet*, we conducted tests using a set of Hyper Suprime-Cam (HSC) exposures, which serve as a precursor to forthcoming imaging data from the Rubin Observatory. The results are highly promising, indicating that the method is well-suited for integration into processing pipelines for studies with ground-based astronomical imaging data.

## 2. Modeling the imaging data

We begin by outlining the setup for our method. Modern astronomical surveys produce datasets consisting of calibrated, co-registered, high-resolution exposures of the same region of the sky, which we denote as  $y = \{y^{(1)}, \dots, y^{(n)}\}$ . For each  $t = 1, \dots, n$ , the image  $y^{(t)} \in \mathbb{R}^d$  is represented as a  $d$ -dimensional column vector, corresponding to a noisy, blurry observation captured at time  $t$ , whose pixel values are denoted as  $y_i^{(t)}$  for  $i = 1, \dots, d$ . To simplify notation, we present the mathematical framework in this paper for images represented as one-dimensional arrays (column vectors). Nonetheless, all models, derivations, and algorithms can be readily adapted and have been implemented for two-dimensional image arrays.

We note that the pixel values  $y_i^{(t)}$  represent photon counts measured at each pixel in each exposure. Along with these measurements, we also obtain auxiliary data on the variability and usability of each pixel value. In particular, we are given corresponding standard deviations  $\sigma_i^{(t)}$ , and hence variances  $v_i^{(t)} \doteq (\sigma_i^{(t)})^2$ , for these measurements. Additionally, each exposure is accompanied by a mask, denoted as  $m = \{m^{(1)}, \dots, m^{(n)}\}$ . The masks are binary arrays indicating whether specific pixel values in the exposures are valid measurements. Specifically, for each  $t = 1, \dots, n$  and  $i = 1, \dots, d$ , the mask entries are defined as follows:

$$m_i^{(t)} \doteq \begin{cases} 1, & \text{if } y_i^{(t)} \text{ is an acceptable measurement,} \\ 0, & \text{otherwise.} \end{cases}$$

Moreover, we are given point-spread functions (PSFs), denoted as  $f = \{f^{(1)}, \dots, f^{(n)}\}$ . For each  $t = 1, \dots, n$ , the PSF  $f^{(t)} \in \mathbb{R}^{d'}$  is a  $d'$ -dimensional column vector (where  $d' < d$ ) that represents the convolution kernel (or blur) associated with exposure  $y^{(t)}$ . These PSFs are typically derived from

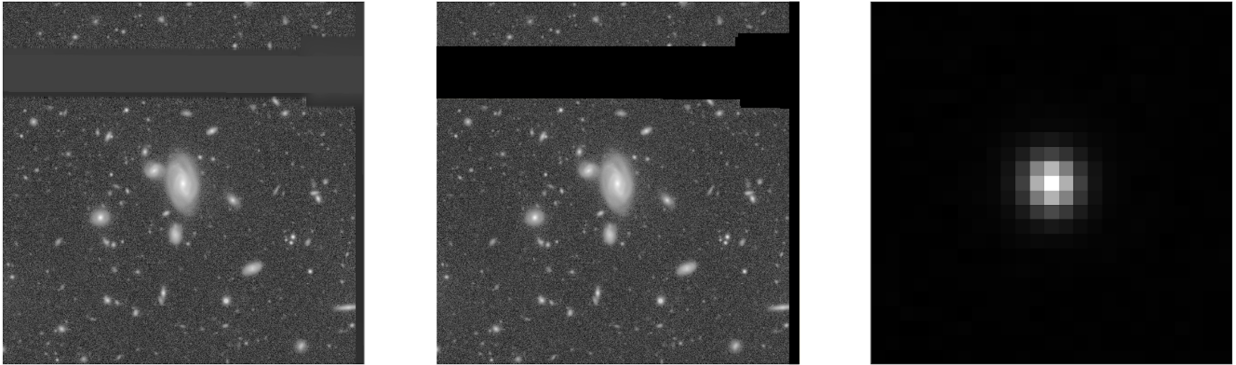


Figure 1: **Hyper Suprime-Cam (HSC) imaging data.** *Left:* A cutout of size  $1000 \times 1000$  pixels from an HSC exposure, where each pixel  $y_i^{(t)}$  is normalized by its standard deviation  $\sigma_i^{(t)}$ . The exposures contain useful information such as sources (e.g. stars, galaxies), which are obfuscated by noise, atmospheric blur and other artifacts, such as occlusions caused by chip gaps and their borders (i.e., the large gray bands with dark gray borders). *Middle:* The masks are applied to each pixel, in order to disregard problematic pixels such as those corresponding to chip gaps and their borders (colored in black). *Right:* The PSF  $f^{(t)}$  for this exposure produced by the HSC software pipeline, of size  $25 \times 25$  pixels (not to scale).

stars in the exposures, which are identified from a catalog of sources.

We display a concrete example of such imaging data in Figure 1, which is sourced from the Hyper Suprime-Cam (HSC) survey. This dataset consists of  $n = 33$  calibrated  $i$ -band exposures taken by the HSC telescope, together with their associated masks and PSFs. For more information on the pre-processing of this imaging data, see [19, 20, 1].

To model the exposures, we follow the approach proposed in the *ImageMM* framework [21]. Specifically, we model each observed exposure  $y^{(t)}$  as the result of convolving the true, background-subtracted, noise-free latent image of the night sky, denoted as  $x$ , with the corresponding PSF  $f^{(t)}$ , plus an additive noise term  $\eta^{(t)}$ . The observed pixel values in each exposure are thus represented by:

$$y_i^{(t)} = (f^{(t)} * x)_i + \eta_i^{(t)}. \quad (1)$$

The noise terms  $\eta_i^{(t)}$  are assumed to be *independently* drawn from a probability distribution with a mean of zero and variance  $v_i^{(t)}$ . For instance, one may model the noise terms as *independent, mean zero Gaussian random variables* whose variances are given by  $v_i^{(t)} \doteq (\sigma_i^{(t)})^2$ , as detailed in [21]. One can also consider noise terms drawn from distributions with heavier tails in order to account for outlier pixel values, as we will explain in the next section.

Moreover, we highlight that in model (1), the PSFs and noise terms may vary between exposures, whereas the underlying latent image of the sky remains *common to all exposures*.

### 3. The AstroClearNet framework

To perform multi-frame astronomical image restoration, our goal is to recover the unknown latent image  $x$  from model (1) using the exposures and PSFs at hand.

#### 3.1. MLE and MAP estimation

A classical approach for doing so involves solving for the latent image  $x$  as a *maximum likelihood estimate* (MLE) of model (1). To do so, one estimates a latent image  $\hat{x}$  which is most likely to have generated the exposures  $y$  and PSFs  $f$ , by maximizing the joint likelihood  $p(x | y, f)$  of the pixel values of  $x$  given the data, i.e., the exposures  $y$  and PSFs  $f$ . Equivalently, the MLE problem entails minimizing the joint negative log-likelihood  $\mathcal{L}(x | y, f) \doteq -\ln p(x | y, f)$  of the latent image's pixel values:

$$\hat{x} = \operatorname{argmin}_{x \in \mathcal{X}} \mathcal{L}(x | y, f). \quad (2)$$

This minimization problem is defined over the set of images with non-negative pixel values, denoted as  $\mathcal{X} \doteq \{x \in \mathbb{R}_+^{d+d'-1}\}$ . Following [21], we enforce this non-negativity constraint to obtain physically meaningful maximum likelihood estimates, where sky pixels are zero and source pixels (e.g., stars, galaxies) have positive values. Additionally, the restored image  $\hat{x}$  is padded with  $d' - 1$  extra pixels to account for flux contributions from sources beyond the telescope's field of view during the restoration process.

However, MLE techniques often fail to form physically meaningful restorations  $\hat{x}$  of the night sky [5, 6, 22]. One may thus operate under a Bayesian framework, and solve for the latent image as a *maximum a posteriori* (MAP) estimate:

$$\hat{x} = \operatorname{argmax}_{x \in \mathcal{X}} \ln p(y, f | x) + \ln p(x). \quad (3)$$

In the formulation above,  $p(y, f | x)$  is the joint conditional distribution of pixel values in the exposures  $y$  and PSFs  $f$  given those in the latent image  $x$ , which is given by the joint distribution of the noise terms from (1) (e.g., the Gaussian distribution). Meanwhile,  $p(x)$  is a prior distribution on the pixels values of the latent image, for which a handcrafted regularization prior, such as the total variation norm [16], might typically be used.

### 3.2. AstroClearNet deep image prior

The key to computing  $\hat{x}$  as a MAP estimate thus lies in an effective choice of regularization prior, which may be challenging in the context of astronomical image restoration. Indeed, the distribution of pixel values in the unknown latent image may be complex, and sometimes indeterminate, especially when working with exposures of unknown regions of the sky. Nevertheless, one can bypass this hurdle and impose an effective prior through the structure of an untrained, generative neural network, i.e., a so-called *deep image prior* [16].

Inspired by this approach, we develop a self-supervised multi-frame method for restoring astronomical images, dubbed *AstroClearNet*. Our approach is an extension of the flash-no flash method for image-pair restoration proposed in [16], to the setting of multi-frame image restoration.

As part of our method, we solve for the latent image in a self-supervised manner using a neural network with an encoder-decoder (i.e., "hourglass") architecture, as illustrated in Figure 2. Similarly to what was outlined in a previous publication by the authors [23], the salient feature of *AstroClearNet* consists of encoding the latent image  $x$  as a *function* of the multiple exposures  $y = \{y^{(1)}, y^{(2)}, \dots, y^{(n)}\}$ . We parametrize this function using a neural network  $F_\theta$  with learnable parameters  $\theta$ . We then decode the latent image  $x = F_\theta(y)$  by convolving it with  $n$  convolutional filters  $f = \{f^{(1)}, \dots, f^{(n)}\}$  in order to produce reconstructions of our input exposures, which we denote by  $\hat{y} = \{\hat{y}^{(1)}, \dots, \hat{y}^{(n)}\}$ , where  $\hat{y}^{(t)} = f^{(t)} * F_\theta(y)$  for

each  $t = 1, \dots, n$ . The convolutional filters  $f$  correspond to the PSFs for each exposure, if these are known. Otherwise, they could be included as additional learnable parameters of the hourglass network, as outlined in Appendix A.

### 3.3. Training the network

Under this setup, the task of solving for the latent image  $x = F_\theta(y)$  boils down to learning the unknown mapping  $F_\theta$ . In turn, this essentially entails tuning the unknown learnable parameters of the network,  $\theta$ , such that the network generates reconstructions  $\hat{y}$  that are consistent with the input exposures  $y$ .

Inspired by the robust restoration framework of [21], we do so by minimizing the *Huber loss* between our network's inputs  $y$  and outputs  $\hat{y}$ , namely:

$$\theta^* = \operatorname{argmin}_\theta \sum_{t,i} m_i^{(t)} H_\delta \left( \frac{y_i^{(t)}}{\sigma_i^{(t)}}, \frac{[f^{(t)} * F_\theta(y)]_i}{\sigma_i^{(t)}} \right) \quad (4)$$

where  $H_\delta : \mathbb{R} \times \mathbb{R} \rightarrow \mathbb{R}$  is defined as follows:

$$H_\delta(y, \hat{y}) := \begin{cases} \frac{1}{2} (y - \hat{y})^2 & \text{for } |y - \hat{y}| \leq \delta, \\ \delta (|y - \hat{y}| - \frac{1}{2}\delta) & \text{otherwise.} \end{cases} \quad (5)$$

We note that  $H_\delta$  is applied pixel-wise across all pairs of corresponding pixels in the input exposures  $y$  and their reconstructions  $\hat{y}$ , which are scaled by their standard deviations. We adopt the Huber loss as it balances sensitivity to small discrepancies and robustness to outliers. Indeed, when the difference between pixel values in  $y$  and  $\hat{y}$  is small (i.e., below a threshold  $\delta \in \mathbb{R}$ ), the Huber loss behaves like the mean squared error, which corresponds to the negative log-likelihood function (2) of the latent image's pixels values under the assumption of Gaussian noise in model (1). However, for larger discrepancies exceeding  $\delta$ , which are typically caused by outlier pixels, the Huber loss transitions to a linear function. This reduces the influence of such outliers on the overall loss, especially compared to the mean squared error. The Huber loss is thus less sensitive to outliers, enabling the recovery of latent images  $\hat{x}$  that are robust to the adverse impact of heavy-tailed noise in the exposures.

For the sake of clarity, we point out that once the network has been trained by finding the optimal network parameter values  $\theta^*$  in (4), the estimated latent image  $\hat{x}$  is then computed via a forward pass through the trained encoder of our hourglass network, namely:

$$\hat{x} = F_{\theta^*}(y). \quad (6)$$

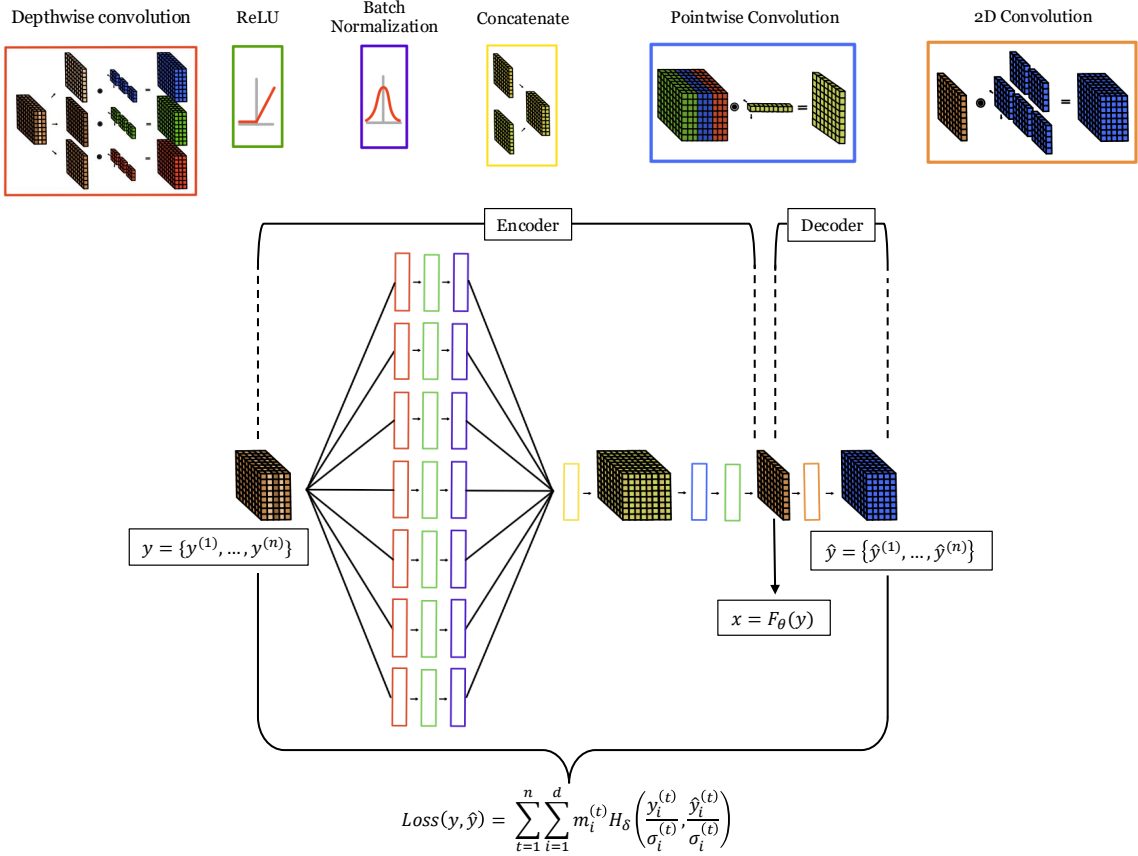


Figure 2: **Network architecture.** The network takes multiple exposures of the night sky  $y = \{y^{(1)}, \dots, y^{(n)}\}$  as input. These exposures pass through the “encoder” of the network, where we extract and combine multi-scale information via various convolutional layers. All input exposures first pass through several depth-wise convolution layers in parallel, before a ReLU activation and batch normalization are applied. The resulting output channels are concatenated, before a pointwise convolution is applied to produce the latent image  $x$ , which respects desired physical constraints such as non-negativity due to the application of another ReLU activation. We then “decode” the latent image  $x$  via a final 2D convolutional layer to produce the reconstructions  $\hat{y} = \{\hat{y}^{(1)}, \dots, \hat{y}^{(n)}\}$ . This last layer corresponds to the PSFs for each exposure (if these are known), and thus contains fixed, constant weights. Otherwise, the weights in the last layer could be considered as additional learnable parameters, allowing for the extension of *AstroClearNet* to the setting of blind multi-frame image restoration, as outlined in Appendix A.

### 3.4. *AstroClearNet* network architecture

We now elaborate on the key architectural features of the *AstroClearNet* neural network, which is illustrated in Figure 2.

- **Hourglass structure:** An hourglass or encoder-decoder architecture naturally fits our image restoration problem. Indeed, since our goal is to recover the latent image  $x$  from the observed exposures based on model (1), we must first map the input exposures into a latent space to learn  $x$ , thus requiring an encoder. The decoder then reconstructs the exposures from the latent image, forming a self-supervised learning framework. This approach is essential, as no labeled training data is available for our task.

- **Multi-frame method and multi-scale feature maps:** Moreover, to effectively learn the latent image, we must combine information from all  $n$  observations. This motivates the use of depthwise convolutions in the encoder. Indeed, unlike traditional convolutions, which aggregate information across input channels, depthwise convolutions apply separate kernels to each channel, thus preserving information specific to each observation. Furthermore, this allows us to capture features at multiple scales by applying depthwise convolutions in parallel with different kernel sizes, promoting the learning of features at varying resolutions. Once the input exposures pass through these depthwise convolution layers, the resulting feature maps are merged using

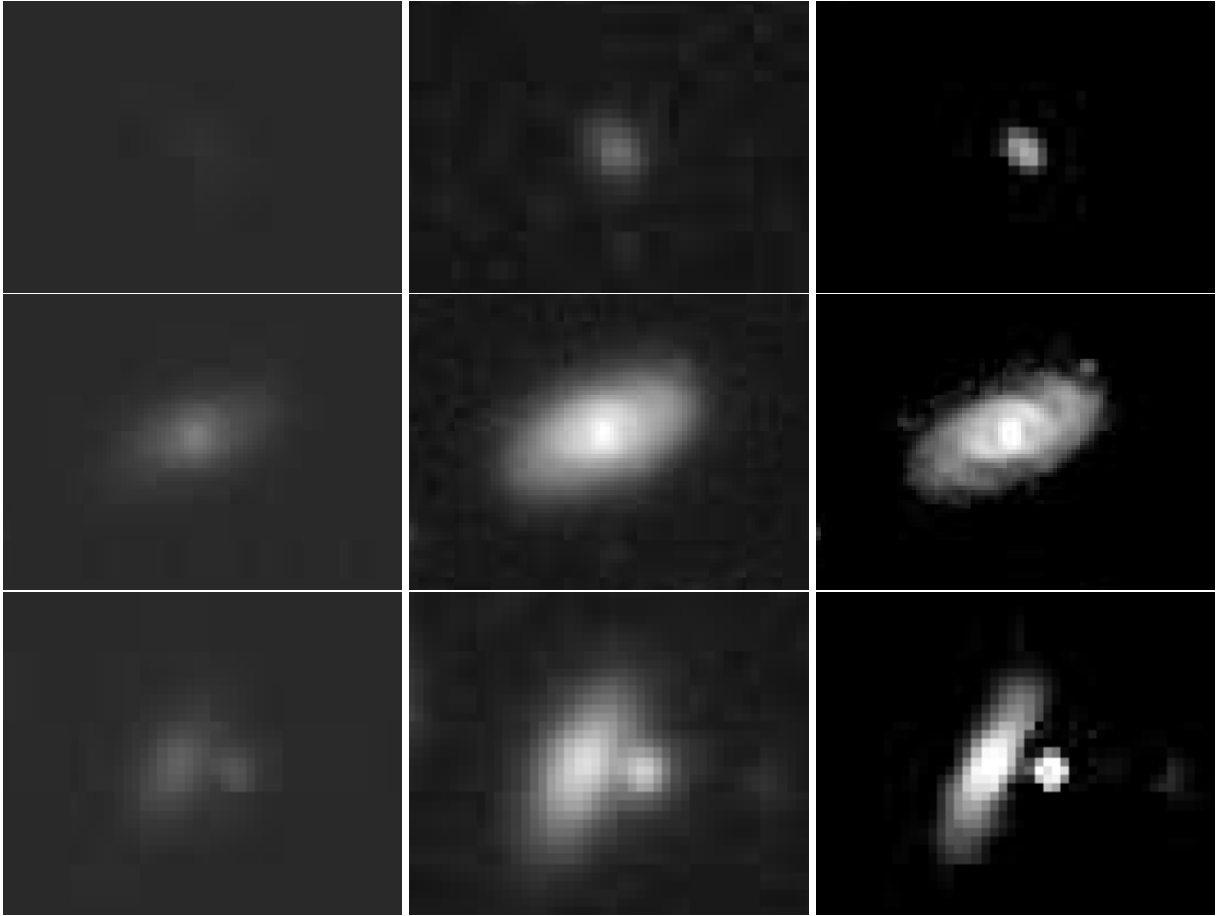


Figure 3: **Results with HSC imaging data.** *Left:* Cutouts from an HSC exposure, where the sky-background is noisy, and blurry sources are hard to detect, especially when they are small and faint (top row). *Middle:* Cutouts from the HSC pipeline coadd, in which sky-background noise is reduced, and sources become more easily distinguishable despite retaining some blur. *Right:* Corresponding cutouts from latent image  $\hat{x}$  obtained using *AstroClearNet*. The estimate  $\hat{x}$  exhibits minimal sky-background noise, and sources appear markedly sharper than those in the coadd, enabling more detailed visualization of fine spatial features such as the shapes and sizes of galaxies (middle and bottom row).

pointwise convolutions, thereby generating a single latent image which combines multi-scale information from all exposures.

• **Incorporating physical model and constraints:** Another key requirement when designing *AstroClearNet* entails ensuring that the network’s output  $\hat{y}$  adheres to the physical model of the exposures given in (1). This principle shapes the decoder’s structure, ensuring that its final layer (a 2D convolution) produces outputs that follow  $\hat{y}^{(t)} = f^{(t)} * x = f^{(t)} * F_{\theta}(y)$  for each  $t = 1, \dots, n$ . By embedding this model directly into the neural network’s architecture, we maintain consistency with the underlying physics. Additionally, to enforce the non-negativity constraint on the latent image

$x$ , we apply a ReLU activation in the last layer of our encoder, thus ensuring the network produces a physically meaningful latent image.

#### 4. Results and discussion

We now present preliminary results obtained by applying *AstroClearNet* on a multi-frame restoration task using ground-based astronomical imaging data from the Hyper Suprime-Cam (HSC) survey, which was described in Figure 1. Specifically, we used  $n = 33$  HSC exposures of size  $4200 \times 4200$  pixels, together with their corresponding masks, standard deviations and PSFs, in order to recover a latent image of the night sky. Our results are presented in Figure 3.

Strikingly, we observe that *AstroClearNet* generates latent images with minimal sky-background noise and noticeably sharper bright sources compared to those in the HSC pipeline coadd. This enhanced clarity reveals fine spatial features—such as the shapes and structures of galaxies—in remarkable detail. We also observe that the method is able to effectively reduce the blur around various types of sources (of various shapes and sizes), even when sources are not well-separated in the exposures.

Despite the overall effectiveness of the approach, certain limitations remain. In particular, the detection of small, low-surface-brightness sources in faint sky regions may be less reliable when using latent images produced by *AstroClearNet*, especially in comparison to advanced multi-frame restoration methods such as *ImageMM* [21]. Further comprehensive photometric evaluations are necessary to rigorously assess the detection limits attainable through *AstroClearNet*’s restorations.

Such limitations suggest several paths for improving on the preliminary results. For instance, it may be possible to enhance the latent images by performing multi-frame image restoration in a higher spatial resolution, as shown in [21, 10]. This would entail modifications of *AstroClearNet*’s network architecture to allow for learning a super-resolved latent image  $x$  with sub-pixel detail in galaxies and stars, which may facilitate the detection of small, faint sources. Moreover, an interesting avenue for future work involves leveraging the differentiability of the network (with respect to the exposures), i.e., the existence of  $\partial_y F_\theta(y)$ , in order to propagate uncertainties from the input exposures through the restoration process. This would allow us to construct confidence intervals for the restored latent images, providing valuable information for subsequent scientific analyses. Furthermore, as part of future work, the authors plan on rigorously comparing *AstroClearNet* with the *ImageMM* method [21], as well as exploring the possibility of combining the two methods to leverage the strengths of each.

## Appendix A. Joint estimation of PSFs

As mentioned in Section 3.2, one can extend the *AstroClearNet* framework in order to perform multi-frame blind image restoration.

In this setting, the PSFs  $f = \{f^{(1)}, \dots, f^{(n)}\}$  corresponding to each exposure  $y = \{y^{(1)}, \dots, y^{(n)}\}$  are assumed to be unknown, and thus, one may jointly estimate the latent image  $x$  and these PSFs  $f$  as

maximum a posterior (MAP) estimates of model (1). This is achieved by computing:

$$\hat{x}, \hat{f} = \operatorname{argmax}_{x, f} \ln p(y | x, f) + \ln p(x, f). \quad (\text{A.1})$$

Note that  $p(y | x, f)$  is the conditional distribution of the pixel values in the exposures  $y$  given those in the latent image  $x$  and PSFs  $f$ , which, as outlined in Section 3.1, is given by the joint distribution of the noise terms from (1) (e.g., the Gaussian distribution). Meanwhile,  $p(x, f)$  is a joint prior distribution on the pixels values of the latent image and PSFs, for which a handcrafted regularization prior is typically used.

Due to the difficulties in coming up with an effective prior, especially in the context of astronomical image restoration, one may therefore compute  $\hat{x}$  and  $\hat{f}$  as MAP estimates by leveraging the *AstroClearNet* deep image prior, exactly as outlined in Section 3.2.

In particular, when training the hourglass network from Figure 2, one would jointly learn the network weights of the encoder,  $\theta$ , as well as the weights of the decoder, i.e., the final 2D convolution layer  $f$ :

$$\theta^*, f^* = \operatorname{argmin}_{\theta, f} \sum_{t, i} m_i^{(t)} H_\delta \left( \frac{y_i^{(t)}}{\sigma_i^{(t)}}, \frac{[f^{(t)} * F_\theta(y)]_i}{\sigma_i^{(t)}} \right) \quad (\text{A.2})$$

The optimal weights of the decoder  $f^*$  obtained after training the network would thus correspond to the MAP estimates of the unknown PSFs for each exposure.

## Acknowledgements

The authors thank Yusra AlSayyad for providing access to the Hyper Suprime-Cam imaging data, and for extending valuable support with regards to the use of the LSST Science Pipelines for processing the data.

Y.S. and F.N. gratefully acknowledge support from the NVIDIA Academic Hardware Grant Program.

T.B. gratefully acknowledges support from the National Science Foundation (Award 1909709).

This research makes use of the SciServer science platform ([www.sciserver.org](http://www.sciserver.org)). SciServer is a collaborative research environment for large-scale data-driven science. It is being developed at, and administered by, the Institute for Data Intensive Engineering and Science at Johns Hopkins University.

SciServer is funded by the National Science Foundation through the Data Infrastructure Building Blocks (DIBBs) program and others, as well as by the Alfred P. Sloan Foundation and the Gordon and Betty Moore Foundation.

## References

- [1] H. Aihara, N. Arimoto, R. Armstrong, S. Arnouts, N. A. Bahcall, S. Bickerton, J. Bosch, K. Bundy, P. L. Capak, J. H. Chan, et al., The hyper supprime-cam ssp survey: overview and survey design, *Publications of the Astronomical Society of Japan* 70 (SP1) (2018) S4.
- [2] Ž. Ivezić, S. M. Kahn, J. A. Tyson, B. Abel, E. Acosta, R. Allsman, D. Alonso, Y. AlSayyad, S. F. Anderson, J. Andrew, et al., Lsst: from science drivers to reference design and anticipated data products, *The Astrophysical Journal* 873 (2) (2019) 111.
- [3] R. N. Tubbs, Lucky exposures: Diffraction limited astronomical imaging through the atmosphere, arXiv preprint astro-ph/0311481 (2003).
- [4] J. Annis, M. Soares-Santos, M. A. Strauss, A. C. Becker, S. Dodelson, X. Fan, J. E. Gunn, J. Hao, Ž. Ivezić, S. Jester, et al., The sloan digital sky survey coadd: 275 deg<sup>2</sup> of deep sloan digital sky survey imaging on stripe 82, *The Astrophysical Journal* 794 (2) (2014) 120.
- [5] T. J. Schulz, Multiframe blind deconvolution of astronomical images, *JOSA A* 10 (5) (1993) 1064–1073.
- [6] Y. V. Zhulina, Multiframe blind deconvolution of heavily blurred astronomical images, *Applied Optics* 45 (28) (2006) 7342–7352.
- [7] S. Harmeling, M. Hirsch, S. Sra, B. Schölkopf, Online blind deconvolution for astronomical imaging, in: 2009 IEEE International Conference on Computational Photography (ICCP), IEEE, 2009, pp. 1–7.
- [8] S. Harmeling, S. Sra, M. Hirsch, B. Schölkopf, Multi-frame blind deconvolution, super-resolution, and saturation correction via incremental em, in: 2010 IEEE International Conference on Image Processing, IEEE, 2010, pp. 3313–3316.
- [9] M. Hirsch, S. Harmeling, S. Sra, B. Schölkopf, Online multi-frame blind deconvolution with super-resolution and saturation correction, *Astronomy & Astrophysics* 531 (2011) A9.
- [10] M. A. Lee, T. Budavári, R. L. White, C. Gulian, Robust statistics for image deconvolution, *Astronomy and computing* 21 (2017) 15–21.
- [11] M. Lee, T. Budavári, Streaming analysis in astronomy: Multiframe blind image deconvolution, *Astronomical Data Analysis Software and Systems XXV* 512 (2017) 199.
- [12] L. Xu, J. S. Ren, C. Liu, J. Jia, Deep convolutional neural network for image deconvolution, *Advances in neural information processing systems* 27 (2014).
- [13] C. J. Schuler, H. Christopher Burger, S. Harmeling, B. Scholkopf, A machine learning approach for non-blind image deconvolution, in: Proceedings of the IEEE conference on computer vision and pattern recognition, 2013, pp. 1067–1074.
- [14] H. Son, S. Lee, Fast non-blind deconvolution via regularized residual networks with long/short skip-connections, in: 2017 IEEE International Conference on Computational Photography (ICCP), IEEE, 2017, pp. 1–10.
- [15] J. Dong, S. Roth, B. Schiele, Deep wiener deconvolution: Wiener meets deep learning for image deblurring, *Advances in Neural Information Processing Systems* 33 (2020) 1048–1059.
- [16] D. Ulyanov, A. Vedaldi, V. Lempitsky, Deep image prior, in: Proceedings of the IEEE conference on computer vision and pattern recognition, 2018, pp. 9446–9454.
- [17] D. Ren, K. Zhang, Q. Wang, Q. Hu, W. Zuo, Neural blind deconvolution using deep priors, in: Proceedings of the IEEE/CVF conference on computer vision and pattern recognition, 2020, pp. 3341–3350.
- [18] M. Asim, F. Shamshad, A. Ahmed, Blind image deconvolution using deep generative priors, *IEEE Transactions on Computational Imaging* 6 (2020) 1493–1506.
- [19] S. Miyazaki, Y. Komiyama, H. Nakaya, Y. Kamata, Y. Doi, T. Hamana, H. Karoji, H. Furusawa, S. Kawanomoto, T. Morokuma, et al., Hyper supprime-cam, in: *Ground-based and Airborne Instrumentation for Astronomy IV*, Vol. 8446, SPIE, 2012, pp. 327–335.
- [20] J. Bosch, R. Armstrong, S. Bickerton, H. Furusawa, H. Ikeda, M. Koike, R. Lupton, S. Mineo, P. Price, T. Takata, et al., The hyper supprime-cam software pipeline, *Publications of the Astronomical Society of Japan* 70 (SP1) (2018) S5.
- [21] Y. Sukurdeep, T. Budavári, A. J. Connolly, F. Navarro, Imagemm: Joint multi-frame image restoration and super-resolution, arXiv preprint arXiv:2501.03002 (2025).
- [22] J.-L. Starck, E. Pantin, F. Murtagh, Deconvolution in astronomy: A review, *Publications of the Astronomical Society of the Pacific* 114 (800) (2002) 1051.
- [23] F. Navarro, D. Hall, T. Budavari, Y. Sukurdeep, Learning the night sky with deep generative priors, arXiv preprint arXiv:2302.02030 (2023).